The structure of a three-dimensional turbulent boundary layer

By A. T. DEGANI[1], F. T. SMITH[2] AND J. D. A. WALKER[1]

[1] Department of Mechanical Engineering and Mechanics, Lehigh University, Bethlehem, PA 18015, USA

[2] Mathematics Department, University College London, London WC1E 6BT, UK

The three-dimensional turbulent boundary layer is shown to have a self-consistent two-layer asymptotic structure in the limit of large Reynolds number. In a streamline coordinate system, the streamwise velocity distribution is similar to that in two-dimensional flows, having a defect-function form in the outer layer which is adjusted to zero at the wall through an inner wall layer. An asymptotic expansion accurate to two orders is required for the cross-stream velocity which is shown to exhibit a logarithmic form in the overlap region. The inner wall-layer flow is collateral to leading order but the influence of the pressure gradient, at large but finite Reynolds numbers, is not negligible and can cause substantial skewing of the velocity profile near the wall. Conditions under which the boundary layer achieves self-similarity and the governing set of ordinary differential equations for the outer layer are derived. The calculated solution of these equations is matched asymptotically to an inner wall-layer solution and the composite profiles so formed describe the flow throughout the entire boundary layer. The effects of Reynolds number and cross-stream pressure gradient on the cross-stream velocity profile are discussed and it is shown that the location of the maximum cross-stream velocity is within the overlap region.

1. Introduction

Three-dimensional turbulent boundary-layer flows are common in nature and in engineering applications. However, it is only in the recent past, with the increasing availability of relatively large computing resources, that a considerable research effort has been expended in devising numerical algorithms and turbulence models for the calculation of such boundary layers. Although much progress has been made in this endeavour, it is fair to say that a basic understanding of the physics and structural features of this flow is not well-established. In a previous study (Degani, Smith & Walker 1992), an asymptotic analysis of the turbulent boundary layer near the plane of symmetry in the limit of large Reynolds number was developed. The latter investigation was carried out as a first step in understanding the general features of the full three-dimensional flow which are now taken up in this study. Here a self-consistent two-layer structure will be shown to describe the attached turbulent boundary layer in three dimensions, with an inner wall layer in which the turbulent and viscous stresses are of comparable magnitude, and a relatively thicker outer layer where the viscous stresses are negligible to leading order.

It is useful at this stage to discuss qualitatively the essential features of a three-dimensional boundary layer, which is most conveniently described in the streamline coordinate system shown schematically in figure 1. Here the coordinates (x_1, x_2) lie on
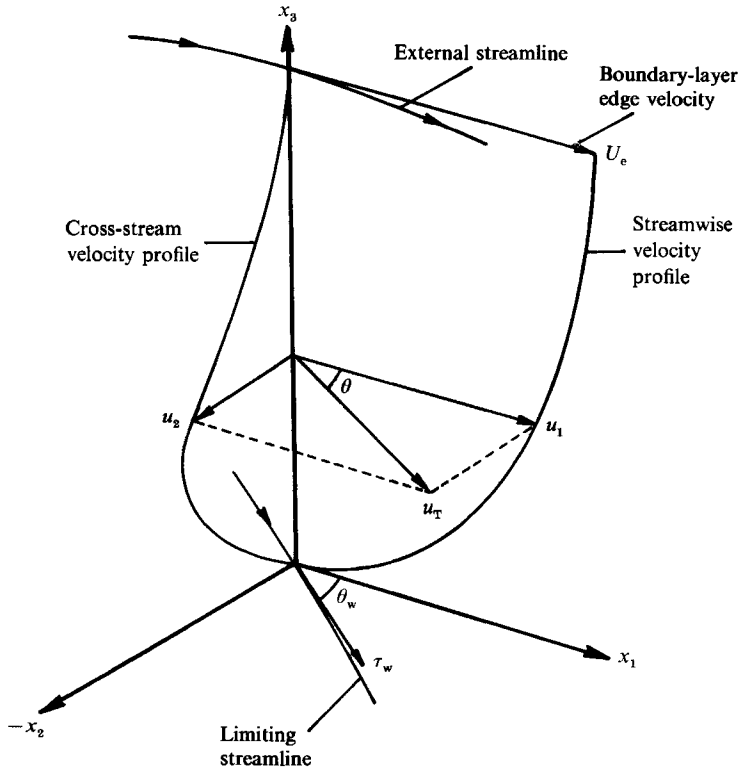
FIGURE 1. Schematic of a three-dimensional turbulent boundary-layer velocity profile.

the surface with x_1 aligned in the direction of the mainstream velocity and x_2 perpendicular to x_1; x_3 is the normal coordinate completing the orthogonal system. In general, the external streamline is curved, which produces a cross-stream pressure gradient that is positive for the situation shown in figure 1. Although the velocity vector, u_T, is tangential to the external streamline at the boundary-layer edge, it tends to rotate in the direction of decreasing cross-stream pressure gradient as the distance from the wall decreases. Thus in the streamline coordinate system, the boundary layer develops a cross-stream velocity component, u_2, the magnitude of which increases from zero at the boundary-layer edge, reaches a maximum value, and then decreases back to zero at the wall in order to satisfy the no-slip condition. On the other hand, the behaviour of the streamwise velocity, u_1, is similar to that in two-dimensional boundary layers. The angle θ between u_T and x_1 is known as the velocity skew angle. Since both u_1 and u_2 are zero at the wall, the wall skew angle, θ_w, is determined by the L'Hôpital rule and consequently θ_w is also the angle between the wall shear stress vector and x_1; it is also the total angle through which the velocity vector rotates as the thickness of the boundary layer is traversed. The total shear stress vector generally has components in each of the (x_1, x_2)-directions and also tends to rotate away from the direction defined by θ_w with increasing distance from the surface.

There are a number of controversial issues concerning three-dimensional turbulent boundary layers which have been discussed by Degani et al. (1992) and Degani (1991). Here only a short summary of the pertinent issues is given.

(i) Although a logarithmic variation with distance from the wall for the streamwise velocity u_1 has been observed in experimental data (Fernholz & Vagt 1981; Van den Berg et al. 1975; Pierce & Zimmerman 1973; Prahlad 1973), the structure of the cross-

stream velocity has not been established yet. A number of 'law of the wall' formulae have been proposed for the cross-stream velocity profile (Pierce, McAllister & Tennant 1983) that contain a logarithmic variation, but this behaviour has not been confirmed experimentally. Furthermore, the nature of the functional form of the cross-stream velocity in the outer layer which matches smoothly with the wall-layer solution has not been addressed. Unlike the streamwise velocity profile, a defect function form for the cross-stream velocity is not possible since u_2 vanishes at the boundary-layer edge. Consequently, both the outer- and wall-layer functional forms for the cross-stream velocity profile remain to be established.

(ii) The extent of near-wall collateral flow reported has varied considerably; here the term collateral flow signifies that the flow is in the same direction as the wall shear stress vector. Some authors (see, for example, Nash & Patel 1972) argue that near-wall collateral flow is inconsistent with the governing equations. In contrast in a recent theoretical study, Goldberg & Reshotko (1984) conclude that the flow is collateral across the entire wall layer. Estimates of the extent of near-wall collateral flow from experimental data vary from $y^+ = 15$ (Johnston 1960) to as high as $y^+ = 150$ (Hornung & Joubert 1963); here $y^+ = u_\tau y/\nu$, where y measures distance normal to the surface, u_τ is the total friction velocity and ν is the kinematic viscosity. At typical Reynolds numbers encountered in practice, the wall-layer thickness extends to about $y^+ \sim 100$. Evidently the extent of collateral flow within the wall layer needs to be established on a theoretical basis.

(iii) The location of the point of maximum cross-stream velocity has also not been determined. Johnston (1960) claimed that the location is well within the wall layer ($y^+ \sim 15$), but Goldberg & Reshotko (1984) suggest that it is within the outer layer. Furthermore, the dependence of this location on the Reynolds number and pressure gradient, if any, has not been established.

(iv) For two-dimensional boundary layers, it is well-known (Fendell 1972) that the appropriate scale for the velocity in the wall layer and the defect function in the outer layer is the friction velocity $u_\tau = (\tau_w/\rho)^{\frac{1}{2}}$, where τ_w is the wall shear stress and ρ is the density. However, a number of possibilities seem to exist for three-dimensional flows. Some of these have been reviewed by Pierce *et al.* (1983) who conclude that the basis of selection of the velocity scale is not clear and remains to be determined.

In order to answer these fundamental questions in a systematic manner, an asymptotic analysis of the governing equations in the limit of large Reynolds number is carried out in the present study. It may be noted that in addition to resolving the fundamental structural questions, the results of an asymptotic analysis are also of considerable practical significance. An important modern trend in the computation of turbulent flow, either by solution methods based on the boundary-layer or full Navier–Stokes equations, is the wall-function method (Rubesin & Viegas 1985; Barnwell, Wahls & DeJarnette 1988; Walker, Ece & Werle 1991). Such approaches in two-dimensional flows are based on the result (Fendell 1972) that the mean wall-layer develops a locally self-similar form; thus the velocity and the total enthalpy in the inner wall layer may be represented by analytical functions in the form of law-of-the-wall profiles. The effectively inviscid flow in the outer layer of the boundary layer is then computed numerically; the no-slip and heat-transfer condition at the wall are replaced by the requirement that the numerical solution asymptote in a manner consistent with the wall-layer structure at numerical mesh points close to the wall (Walker *et al.* 1991). Since this approach obviates the necessity of obtaining a numerical solution near the wall, where ordinarily a highly refined mesh is needed to resolve the intense profile gradients, a considerable saving in mesh points and computational time is possible. For

instance, in a recent paper on the calculation of two-dimensional boundary-layer flow with heat transfer (Walker *et al.* 1991) it was shown that a 50% reduction in the number of mesh points – as compared to that required for a conventional calculation which computes the flow all the way to the wall – was possible without any degradation in accuracy. Recently, the basic approach has been extended to attached three-dimensional flows using the theory developed in this study (Degani 1991; Degani & Walker 1991), where pay-offs in increased computing efficiency are much more significant. In order to specify the asymptotic boundary condition for the outer-layer numerical solution and the appropriate form of the wall functions, it is first necessary to determine a complete and self-consistent structure for the three-dimensional turbulent boundary layer.

In the context of the brief foregoing background, the objectives of the present study may be summarized as follows:

(i) to develop the asymptotic structure of the three-dimensional turbulent boundary layer in the limit of large Reynolds number;

(ii) to determine the conditions that the external flow must satisfy for the boundary layer to achieve self-similarity, thus providing the three-dimensional analogue of the two-dimensional boundary layer (Clauser 1954, 1956);

(iii) to obtain similarity solutions of the three-dimensional turbulent boundary layer to facilitate the discussion of some general features of the flow.

2. Governing equations

Consider a three-dimensional boundary-layer flow and let U_{ref} and L_{ref} be a representative speed and length, respectively; the Reynolds number is defined as $Re = U_{\text{ref}} L_{\text{ref}}/\nu$, where ν is the kinematic viscosity. In dimensionless variables, the Reynolds-averaged boundary-layer equations in a streamline coordinate system are

$$\frac{\partial}{\partial x_1}(h_2 u_1) + \frac{\partial}{\partial x_2}(h_1 u_2) + h_1 h_2 \frac{\partial u_3}{\partial x_3} = 0, \tag{2.1}$$

$$\frac{u_1}{h_1}\frac{\partial u_1}{\partial x_1} + \frac{u_2}{h_2}\frac{\partial u_1}{\partial x_2} + u_3 \frac{\partial u_1}{\partial x_3} - K_2 u_1 u_2 + K_1 u_2^2 = \frac{U_e}{h_1}\frac{\partial U_e}{\partial x_1} + \frac{\partial \tau_{13}}{\partial x_3}, \tag{2.2}$$

$$\frac{u_1}{h_1}\frac{\partial u_2}{\partial x_1} + \frac{u_2}{h_2}\frac{\partial u_2}{\partial x_2} + u_3 \frac{\partial u_2}{\partial x_3} - K_1 u_1 u_2 + K_2 u_1^2 = K_2 U_e^2 + \frac{\partial \tau_{23}}{\partial x_3}, \tag{2.3}$$

where the x_i are as shown in figure 1 and u_i is the velocity in the x_i-direction. The metric coefficients in the streamwise and cross-stream directions are h_1 and h_2, respectively, and K_1 and K_2 are the curvatures defined by

$$K_1 = -\frac{1}{h_1 h_2}\frac{\partial h_2}{\partial x_1}, \quad K_2 = -\frac{1}{h_1 h_2}\frac{\partial h_1}{\partial x_2}. \tag{2.4a, b}$$

In accordance with conventional boundary-layer theory (Nash & Patel 1972), the metric coefficient in the normal direction h_3 is taken equal to unity and h_1 and h_2 are assumed independent of x_3. Lastly, τ_{13} and τ_{23} are the total shear stresses in the x_1- and x_2-directions, respectively, and are given by

$$\tau_{i3} = \sigma_{i3} + \frac{1}{Re}\frac{\partial u_i}{\partial x_3}, \quad i = 1, 2, \tag{2.5}$$

where σ_{i3} are the dimensionless Reynolds stresses.

In the streamline coordinate system,

$$u_1 \to U_e(x_1, x_2), \quad u_2 \to 0, \qquad (2.6a, b)$$

at the boundary-layer edge, where U_e is the flow speed along external streamlines near the surface. In addition to U_e, it is also necessary to specify the function $q(x_1, x_2)$ defined by

$$qU_e = \operatorname*{Lim}_{x_3 \to 0} \frac{\partial U_{3e}}{\partial x_3}, \qquad (2.7)$$

where U_{3e} denotes the normal velocity in the external flow, in order to completely characterize the nature of the mainstream flow near the surface. Assuming that the component of vorticity normal to the surface is zero, it is easily shown that $h_1 = 1/U_e$, and, from the continuity equation (2.1), it follows that the cross-stream metric satisfies

$$K_1 = -\frac{U_e}{h_2} \frac{\partial h_2}{\partial x_1} = \frac{\partial U_e}{\partial x_1} + q. \qquad (2.8)$$

Note that for the special case $q = 0$ (corresponding to inviscid flows which are effectively independent of x_3 near the surface), it follows that $h_2 = 1/U_e$ also. In general for $q \neq 0$, (2.8) defines a differential equation for h_2 which may be integrated along individual streamlines (for known q and U_e).

3. Asymptotic analysis

The turbulent boundary layer is known to be double-structured for both the two-dimensional flow (Yajnik 1970; Fendell 1972; Mellor 1972) and plane-of-symmetry flow (Degani *et al.* 1992). Similar results are expected for the fully three-dimensional flow and here a two-layer structure is sought which is self-consistent in the limit of large Reynolds number.

The friction velocity is defined in the usual manner by $u_\tau = \tau_w^{\frac{1}{2}}$, where τ_w is the non-dimensional magnitude of the wall shear stress. The wall skew angle θ_w is given by

$$\tan \theta_w = \tau_{23}/\tau_{13} \quad \text{at} \quad x_3 = 0, \qquad (3.1)$$

while the scaled outer and inner variables, η and y^+, respectively, are defined by

$$\eta = x_3/\Delta_o, \quad y^+ = x_3/\Delta_i, \quad \Delta_i = (Re\, u_\tau)^{-1}. \qquad (3.2a, b)$$

Here Δ_o is representative of the outer-layer thickness and is $O(u_\tau)$. Note that the definitions of y^+ and Δ_i are identical to those in two-dimensional (Fendell 1972) and plane-of-symmetry (Degani *et al.* 1992) turbulent boundary layers. Finally, two pressure-gradient parameters, defined as

$$\beta_s = \frac{\Delta_o}{U_e u_\tau} \frac{1}{h_1} \frac{\partial p_e}{\partial x_1}, \quad \beta_n = \frac{\Delta_o}{U_e u_\tau} \frac{1}{h_2} \frac{\partial p_e}{\partial x_2}, \qquad (3.3a, b)$$

are of importance in the present study; here the streamwise and cross-stream pressure gradients are given by

$$\frac{1}{h_1} \frac{\partial p_e}{\partial x_1} = -\frac{U_e}{h_1} \frac{\partial U_e}{\partial x_1}, \quad \frac{1}{h_2} \frac{\partial p_e}{\partial x_2} = -K_2 U_e^2 = -\frac{U_e}{h_2} \frac{\partial U_e}{\partial x_2}. \qquad (3.4a, b)$$

First consider the wall layer. Since the total shear stresses in the streamwise and cross-stream directions at the wall are $u_\tau^2 \cos \theta_w$ and $u_\tau^2 \sin \theta_w$, respectively, the following expansions for the total shear stress in the wall layer are suggested:

$$\tau_{13} = u_\tau^2 \cos \theta_w(\bar{x}; Re)\, \tau_1(\bar{x}, y^+) + \dots, \quad \tau_1 = 1 \quad \text{at} \quad y^+ = 0, \qquad (3.5a, b)$$

$$\tau_{23} = u_\tau^2 \sin \theta_w(\bar{x}; Re)\, \tau_2(\bar{x}, y^+) + \dots, \quad \tau_2 = 1 \quad \text{at} \quad y^+ = 0, \qquad (3.5c, d)$$

where $\bar{x}$ denotes (x_1, x_2). The turbulent shear stresses are expected to be the dominant parts of the total shear stress for large y^+ and are therefore expanded according to

$$\sigma_{13} = u_\tau^2 \cos\theta_w(\bar{x}; Re)\, \sigma_1(\bar{x}, y^+) + \dots, \quad \sigma_1 = 0 \quad \text{at} \quad y^+ = 0, \qquad (3.6a, b)$$

$$\sigma_{23} = u_\tau^2 \sin\theta_w(\bar{x}; Re)\, \sigma_2(\bar{x}, y^+) + \dots, \quad \sigma_2 = 0 \quad \text{at} \quad y^+ = 0. \qquad (3.6c, d)$$

Upon substituting (3.5) and (3.6) into (2.5), it follows that the velocities in the streamwise and cross-stream directions have the expansions

$$u_1 = u_\tau \cos\theta_w(\bar{x}; Re)\, U^+(\bar{x}, y^+) + \dots, \quad u_2 = u_\tau \sin\theta_w(\bar{x}; Re)\, \Omega^+(\bar{x}, y^+) + \dots.$$
$$(3.7a, b)$$

Here the profile functions U^+ and Ω^+ are such that

$$U^+ = \Omega^+ = 0 \quad \text{at} \quad y^+ = 0, \qquad (3.8)$$

to satisfy the no-slip condition, and due to the definition of $\varDelta_i$ in (3.2), it follows that

$$\partial U^+/\partial y^+ = \partial \Omega^+/\partial y^+ = 1 \quad \text{at} \quad y^+ = 0. \qquad (3.9)$$

Next, consider the streamwise and cross-stream momentum equations (2.2) and (2.3). Upon substitution of the expansions in (3.5)–(3.7), it is easily verified that

$$u_\tau^2 \cos\theta_w \frac{\partial \tau_1}{\partial y^+} = O\left(\frac{1}{Re\, u_\tau}\right), \quad u_\tau^2 \sin\theta_w \frac{\partial \tau_2}{\partial y^+} = O\left(\frac{1}{Re\, u_\tau}\right), \qquad (3.10a, b)$$

in the wall layer. It will be shown subsequently that

$$\frac{1}{Re\, u_\tau^3 \cos\theta_w} \to 0, \quad \frac{1}{Re\, u_\tau^3 \sin\theta_w} \to 0 \quad \text{as} \quad Re \to \infty. \qquad (3.11a, b)$$

Consequently the total shear stress is constant in magnitude and direction throughout the wall layer and from (3.5),

$$\tau_1 = \tau_2 = 1, \qquad (3.12)$$

for all y^+. Substitution of (3.5)–(3.7) in (2.5) then yields

$$\sigma_1 + \partial U^+/\partial y^+ = 1, \quad \sigma_2 + \partial \Omega^+/\partial y^+ = 1. \qquad (3.13a, b)$$

It may be noted that (3.13b) is identically satisfied if

$$\sigma_2 = \sigma_1, \quad \Omega^+ = U^+, \qquad (3.14a, b)$$

implying that, to leading order, the flow in the wall layer is collateral, a conclusion also reached for the flow in the plane of symmetry (Degani *et al.* 1992). This indicates that the wall-layer flow, in a plane defined by the direction of the wall shear stress and the normal to the wall, is identical to that in a two-dimensional flow to leading order. Therefore, the asymptotic form of U^+ in the limit of large y^+ is given by

$$U^+ \sim \frac{1}{\kappa}\log y^+ + C_i \quad \text{as} \quad y^+ \to \infty, \qquad (3.15)$$

where κ and C_i are the von Kármán and log-law constants and assumed to be given by $\kappa = 0.41$ and $C_i = 5.0$. Equations (3.7), (3.14) and (3.15) are equivalent to the three-dimensional 'law of the wall' originally proposed by Johnston (1960). Note in passing that models for the cross-flow equation in the wall layer other than those in (3.14) are mathematically possible, but are believed to be physically unrealistic for the following reason. If the Reynolds stress σ_2 is arbitrarily specified (subject to condition (3.6a)),

it follows that $\partial \Omega^{+}/\partial y^{+}$ is completely determined from (3.13b). However, such possibilities generally imply a flow in which the velocity, velocity gradient, and Reynolds stress vectors have different skew angles throughout the wall layer and are not aligned with the total stress vector except at the wall itself. However, the convective and pressure-gradient terms in the momentum equations do not influence the leading-order wall-layer solution, and the dominant influence on the near-wall flow is the wall shear stress. Consequently such models do not appear to be realistic in the limit $Re \to \infty$ as the wall-layer thickness shrinks to zero. However, it must be emphasized, as illustrated in §7, that higher-order effects associated with the pressure gradient are not negligible in the near-wall flow for finite Reynolds numbers and may cause the velocity and shear stress profiles to skew in the wall layer. Consequently the leading-order solution adopted in (3.14) does not imply that the wall-layer flow is collateral to all orders, as previously suggested by Goldberg & Reshotko (1984).

Now consider a defect-function formulation for the streamwise velocity in the outer layer. It may be easily confirmed that in order to match the wall-layer expansion, the streamwise velocity in the outer layer must be expanded according to

$$u_1 = U_e + u_\tau \cos \theta_w \frac{\partial F_1}{\partial \eta}(\bar{x}, \eta) + \ldots, \tag{3.16}$$

where the defect function behaves according to

$$\frac{\partial F_1}{\partial \eta} \sim \frac{1}{\kappa} \log \eta + C_0 \quad \text{as} \quad \eta \to 0, \quad \frac{\partial F_1}{\partial \eta} \to 0 \quad \text{as} \quad \eta \to \infty, \tag{3.17a, b}$$

with the resulting velocity-match condition given by

$$\frac{1}{u_*} = \frac{1}{\kappa} \log (Re \, u_\tau \, \Delta_0) + C_i - C_0 + \ldots. \tag{3.18}$$

Here the small parameter u_* is defined by

$$u_* = (u_\tau/U_e) \cos \theta_w, \tag{3.19}$$

and (3.18) establishes a relation between u_*, Re and the outer lengthscale Δ_0; it is evident that u_* is $O(1/\log Re)$ as $Re \to \infty$.

The expansion of the streamwise velocity given by (3.16) indicates that within the outer layer, the deviation from the boundary-layer edge value is of $O(u_*)$. To establish the order of magnitude of the cross-stream velocity in the outer layer, consider (3.7b) and (3.14); using the asymptotic form (3.15) and the matching condition (3.18), it is easily shown that

$$u_2 \sim U_e \tan \theta_w + u_\tau \sin \theta_w \left\{ \frac{1}{\kappa} \log \eta + C_0 \right\} + \ldots \quad \text{as} \quad \eta \to 0, \tag{3.20}$$

in order to ensure an overlap with the wall-layer solution. However, as indicated by (3.16), the defect in the outer layer is $O(u_\tau \cos \theta_w)$, and the cross-stream velocity is expected to be of comparable magnitude. Balancing the leading term in (3.20) with $u_\tau \cos \theta_w$ shows that $\tan \theta_w$ is $O(u_*)$. This result is in agreement with that obtained for the flow near the plane of symmetry (Degani *et al.* 1992) and shows that θ_w is small, in general, in the limit $Re \to \infty$; note that (3.11) is now confirmed.

A scaled wall skew angle θ_* may formally be defined by

$$\theta_* = \tan (\theta_w)/u_*, \tag{3.21}$$

for which θ_* is $O(1)$. It may be noted that since θ_w is small, (3.21) may be written as $\theta_* = \theta_w/u_*$ to leading order; however, there is no special advantage to expanding the trigonometric functions in a Taylor series in the subsequent analysis. In terms of θ_*, the wall-layer expansions of the Reynolds shear stress and velocity given by (3.6) and (3.7), may be rewritten as

$$\sigma_{13} = u_\tau^2 \cos\theta_w \, \sigma_1 + \ldots, \quad \sigma_{23} = u_\tau^2 \cos\theta_w (u_* \theta_*) \, \sigma_1 + \ldots, \qquad (3.22a, b)$$

$$u_1 = U_e u_* U^+ + \ldots, \quad u_2 = U_e u_*^2 \theta_* U^+ + \ldots, \qquad (3.22c, d)$$

where (3.14) has been used. It is important to note that the cross-stream quantities are smaller than their streamwise counterparts by $O(u_*)$. Degani (1991) has considered higher-order terms in the expansions and has shown that these are associated with the pressure gradient and are $O(1/(Re u_*))$ and $O(1/Re u_*^2)$ for the shear stress and velocity, respectively. It is these higher-order terms which cause the shear stress and velocity profiles to deviate at finite Reynolds number from the leading-order collateral flow behaviour described by (3.22). The details of the higher-order analysis are not important for the present purposes and are not included here.

For the outer layer, (3.20) and (3.21) suggest that the appropriate asymptotic expansion for the cross-stream velocity is given by

$$u_2 = U_e u_* \theta_* \left\{ \frac{\partial G_1}{\partial \eta} + u_* \frac{\partial G_2}{\partial \eta} + \ldots \right\}, \qquad (3.23)$$

where $$\frac{\partial G_1}{\partial \eta} \sim 1, \quad \frac{\partial G_2}{\partial \eta} \sim \frac{1}{\kappa}\log\eta + C_0 \quad \text{as} \quad \eta \to 0. \qquad (3.24a, b)$$

It may be inferred that the characteristic 'bulge' in the cross-stream velocity profile is a direct consequence of the asymptotic form in (3.24). At the outer edge of the boundary layer, u_2 is dominated by the leading-order term in (3.23) which increases in magnitude as η decreases. However, very close to the wall layer the logarithmic variation in the second-order term begins to make an increasing (negative) contribution to the cross-stream velocity and at some location within the logarithmic zone (to be estimated in §7), the cross-stream velocity attains its maximum. Below the location of the maximum velocity, the logarithmic term is increasingly dominant and serves to reduce the sum of the $O(u_*)$ and $O(u_*^2)$ terms in the cross-stream velocity to $O(u_*^2)$ in the wall layer, thus enabling a match of the outer-layer and wall-layer expansions (cf. (3.22d)). Consequently, it is not necessary to introduce an empirical profile to obtain the desired cross-stream behaviour as suggested by Goldberg & Reshotko (1984).

As indicated by (3.23), the asymptotic analysis must be extended to second order in the outer layer. The following extension of the expansion in (3.16) is suggested:

$$u_1 = U_e \left\{ 1 + u_* \frac{\partial F_1}{\partial \eta} + u_*^2 \frac{\partial F_2}{\partial \eta} + \ldots \right\}, \qquad (3.25)$$

where the asymptotic form for $\partial F_1/\partial\eta$ is given by (3.17) and $\partial F_2/\partial\eta$ asymptotes as

$$\partial F_2/\partial\eta \sim C_1 \quad \text{as} \quad \eta \to 0. \qquad (3.26)$$

The quantities C_0 and C_1 in (3.17) and (3.26) are functions of $\bar{x}$ which are to be found and which generally depend on the specific outer-layer turbulence model. The asymptotic form in (3.26) is not obvious and merits explanation. In past analyses (Mellor 1972; Goldberg & Reshotko 1984), the flow quantities were expanded in powers of ϵ, where $\epsilon = \epsilon(Re)$ and ϵ is $O(u_\tau)$ at some representative station along the

surface. A logarithmic asymptotic form for $\partial F_2/\partial \eta$ was proposed and this in turn required a term for u_1 which is $O(\epsilon^2)$ in the wall layer. However, in this study, the expansion for the wall-layer velocity is in terms of the friction velocity $u_\tau(x, Re)$ and, consequently, the entire logarithmic variation in u_1 is captured by the leading-order terms in both the outer and wall layers. It has been shown (Degani 1991) that the second term in the expansion for the velocity in the wall layer is of $O(1/(Re\, u_*^2))$, and, consequently, a logarithmic variation in η in (3.26) is incompatible with the wall-layer expansion. This point is amplified in detail in Degani (1991) where it has been shown that an expansion in ϵ, when expressed in terms of an expansion in the friction velocity, produces the result in (3.26). Upon matching (3.22c) and (3.25), it is readily confirmed that the match condition up to second order is

$$\frac{1}{u_*} = \frac{1}{\kappa}\log\left(Re\, u_\tau \varDelta_0\right) + C_i - C_0 - u_* \, C_1 \ldots. \tag{3.27}$$

Now consider the form of the higher-order terms for the total shear stress. Starting with the wall layer, (3.22c, d) are substituted into the momentum equations (2.2) and (2.3). It follows from differentiation of (3.27) that $\partial u_*/\partial x_1$ and $\partial u_*/\partial x_2$ are both $O(u_*^2)$, and upon using (2.1) and (3.2), it is easily shown that

$$\frac{\partial \tau_{13}}{\partial y^+} = -\frac{1}{Re\, u_\tau}\left\{\frac{U_e}{h_1}\frac{\partial U_e}{\partial x_1} - u_*^2\left\{\frac{U_e}{h_1}\frac{\partial U_e}{\partial x_1}U^{+2} + K_1\, U_e^2\frac{dU^+}{dy^+}\int_0^{y^+} U^+\, dy^+\right\}\right\} + \ldots, \tag{3.28}$$

$$\frac{\partial \tau_{23}}{\partial y^+} = -\frac{1}{Re\, u_\tau}\{K_2\, U_e^2\{1 - u_*^2\, U^{+2}\}\} + \ldots. \tag{3.29}$$

The values of τ_{13} and τ_{23} at the wall are $u_\tau^2 \cos\theta_w$ and $u_\tau^2 \cos\theta_w(u_* \, \theta_*)$, respectively, and (3.28) and (3.29) may be integrated from the wall; subsequent evaluation of these expressions for large y^+ yields

$$\tau_{13} \sim u_\tau^2 \cos\theta_w - \frac{1}{Re\, u_\tau}\frac{U_e}{h_1}\frac{\partial U_e}{\partial x_1}y^+\left\{1 - u_*^2\frac{\log^2 y^+}{\kappa^2}\right\} + \ldots \quad \text{as} \quad y^+ \to \infty, \tag{3.30}$$

$$\tau_{23} \sim u_\tau^2 \cos\theta_w\, u_* \, \theta_* - \frac{1}{Re\, u_\tau}K_2\, U_e^2 y^+\left\{1 - u_*^2\frac{\log^2 y^+}{\kappa^2}\right\} + \ldots \quad \text{as} \quad y^+ \to \infty, \tag{3.31}$$

where (3.15) has been used. Note that the second-order terms in (3.30) and (3.31) involve the pressure gradient and act to alter the leading-order collateral flow behaviour in the wall layer for finite Reynolds number.

For the outer layer, it may be confirmed using condition (3.27) that in order to match (3.30), τ_{13} must have the outer-layer expansion

$$\tau_{13} = u_\tau^2 \cos\theta_w\{T_1(\bar{x}, \eta) + u_* \, T_2(\bar{x}, \eta) + \ldots\}. \tag{3.32}$$

Here
$$T_1 \sim 1 - 2\beta_s\frac{\eta\log\eta}{\kappa} + \ldots, \quad T_2 \sim -\beta_s\frac{\eta\log^2\eta}{\kappa^2} + \ldots \quad \text{as} \quad \eta \to 0, \tag{3.33a, b}$$

where β_s is given by (3.3a). Similarly, the appropriate expansion for τ_{23} in the outer layer is

$$\tau_{23} = u_\tau^2 \, \theta_* \cos\theta_w\{\tilde{T}_1(\bar{x}, \eta) + u_* \, \tilde{T}_2(\bar{x}, \eta) + \ldots\}, \tag{3.34}$$

with
$$\tilde{T}_1 \sim 2\gamma\frac{\eta\log\eta}{\kappa} + \ldots, \quad \tilde{T}_2 \sim 1 + \gamma\frac{\eta\log^2\eta}{\kappa^2} + \ldots \quad \text{as} \quad \eta \to 0, \tag{3.35a, b}$$

where the parameter γ is defined in terms of the cross-stream pressure-gradient parameter β_n according to

$$\gamma = -\beta_n/\theta_*, \tag{3.36}$$

and β_n is given by (3.3b). It is important to note that (3.32)–(3.35) are general results that must hold for any turbulence model adopted.

4. Outer-layer similarity equations

In this section, the special case of self-similar flow will be considered as an example of the application of the general theory; this represents a limit in which the number of independent variables is reduced from three to one. It will be subsequently shown that the parameters β_s and β_n defined by (3.3) define a two-parameter family of self-similar flows in a manner similar to that near a plane of symmetry (Degani *et al.* 1992).

Consider two functions ψ and ϕ defined by

$$u_1 = \frac{1}{h_2} \frac{\partial \psi}{\partial x_3}, \quad u_2 = \frac{1}{h_1} \frac{\partial \phi}{\partial x_3}. \tag{4.1 a, b}$$

From the continuity equation (2.1), it follows that

$$u_3 = -\frac{1}{h_1 h_2} \frac{\partial \psi}{\partial x_1} - \frac{1}{h_1 h_2} \frac{\partial \phi}{\partial x_2}. \tag{4.2}$$

The expansions of the velocity in the outer layer given by (3.23) and (3.25) indicate the following expansions for ψ and ϕ:

$$\psi = U_e h_2 \varDelta_0 \{\eta + u_* F_1(\eta) + u_*^2 F_2(\eta) + \ldots\}, \tag{4.3 a}$$

$$\phi = U_e h_1 \varDelta_0 u_* \theta_* \{G_1(\eta) + u_* G_2(\eta) + \ldots\}. \tag{4.3 b}$$

Equations (4.1)–(4.3) and the expansions (3.32) and (3.34) for the total shear stresses are substituted into the momentum equations (2.2) and (2.3) to obtain the similarity equations accurate to first and second order in u_*. For this purpose, it is necessary to evaluate the gradients of u_*; upon differentiation of (3.27), it may be shown that

$$\frac{1}{h_1} \frac{\partial u_*}{\partial x_1} = \frac{1}{\kappa} \frac{u_*^3}{\varDelta_0} (\beta_s - \alpha_s) + O(u_*^3) \ldots, \quad \frac{1}{h_2} \frac{\partial u_*}{\partial x_2} = \frac{1}{\kappa} \frac{u_*^3}{\varDelta_0} (\beta_n - \alpha_n) + O(u_*^3) + \ldots. \tag{4.4 a, b}$$

Here β_s and β_n are given in (3.3) and the quantities α_s and α_n are defined as

$$\alpha_s = \frac{U_e}{u_\tau} \frac{1}{h_1} \frac{\partial \varDelta_0}{\partial x_1}, \quad \alpha_n = \frac{U_e}{u_\tau} \frac{1}{h_2} \frac{\partial \varDelta_0}{\partial x_2}. \tag{4.5 a, b}$$

Along with the parameters β_s, β_n, α_s, α_n and γ (defined in (3.36)), three additional parameters appear in the similarity equations and are defined as follows:

$$\nu = q U_e \varDelta_0/u_\tau, \tag{4.6}$$

$$\lambda_s = \frac{\varDelta_0 U_e}{u_\tau} \frac{1}{\theta_* h_1} \frac{\partial \theta_*}{\partial x_1}, \quad \lambda_n = \frac{u_e \varDelta_0}{u_\tau} \frac{1}{h_2} \frac{\partial \theta_*}{\partial x_2}, \tag{4.7 a, b}$$

where q is defined in (2.7). Since the analysis here is carried out to two orders, it is necessary to account for the fact that some of the parameters listed may have expansion in powers of u_*. A convenient choice for $\varDelta_0$ will be made subsequently (see

(4.20) below) and hence the quantities β_s, β_n and ν may be considered fixed definitions. On the other hand, the parameter γ (cf. (3.36)) involves the wall skew angle and is expected to involve contributions from both the first- and second-order profiles; thus γ is expanded as

$$\gamma = \gamma_0 + u_* \gamma_1 + \dots, \tag{4.8}$$

and from (3.36) the scaled wall skew angle has the expansion

$$\theta_* = -\frac{\beta_n}{\gamma_0} + u_* \left(\frac{\beta_n \gamma_1}{\gamma_0^2}\right) + \dots. \tag{4.9}$$

In addition, since α_s and α_n both contain gradients of Δ_0 they are expanded as

$$\alpha_s = \alpha_{s0} + u_* \alpha_{s1} + \dots, \quad \alpha_n = \alpha_{n0} + u_* \alpha_{n1} + \dots. \tag{4.10a, b}$$

In these expansions, $u_* = u_*(\bar{x}, Re)$ but, upon substitution in the momentum equations (2.2) and (2.3), it may be verified (after some algebra) that the coefficients in the expansions (4.9)–(4.10), as well as β_s, β_n and ν, must all be constant to ensure self-similarity. It then follows from (4.4), (4.7) and (4.9) that $\lambda_s, \lambda_n = O(u_*^2)$.

The first-order streamwise and cross-stream equations may be shown to be

$$T_1' + (\alpha_{s0} - \nu)\eta F_1'' + 2\beta_s F_1' = 0, \tag{4.11}$$

$$\tilde{T}_1' + (\alpha_{s0} - \nu)\eta G_1'' + \nu G_1' = 2\gamma_0 F_1', \tag{4.12}$$

while the second-order equations are

$$T_2' + (\alpha_{s0} - \nu)\eta F_2'' + 2\beta_s F_2' = Z_1, \tag{4.13}$$

$$\tilde{T}_2' + (\alpha_{s0} - \nu)\eta G_2'' + \nu G_2' = Z_2, \tag{4.14}$$

where the primes denote differentiation with respect to η. The right-hand sides of (4.13) and (4.14) are given by

$$Z_1 = -\frac{\alpha_{s0} - \beta_s}{\kappa} F_1' - \alpha_{s1} \eta F_1'' - (\alpha_{s0} - \nu) F_1 F_1'' - \beta_s (F_1')^2 + \frac{\beta_n \alpha_{n0}}{\gamma_0} G_1 F_1'' - (\beta_s - \nu)\frac{\beta_n^2}{\gamma_0^2}(G_1')^2, \tag{4.15}$$

and

$$Z_2 = 2\gamma_0 F_2' + 2\gamma_1 F_1' - \frac{\alpha_{s0} - \beta_s}{\kappa} G_1' - \alpha_{s1} \eta G_1'' - \nu F_1' G_1' - (\alpha_{s0} - \nu) F_1 G_1''$$

$$+ \frac{\beta_n \alpha_{n0}}{\gamma_0} G_1 G_1'' + \frac{\beta_n^2}{\gamma_0}(G_1')^2 + \gamma_0 (F_1')^2. \tag{4.16}$$

Not all the constants in (4.11)–(4.16) are independent and connecting relationships are now obtained.

Unlike two-dimensional flow, the definition of a displacement thickness in three-dimensional flow is ambiguous (see, for example, Nash & Patel 1972). However, a lengthscale δ^*, which is rotationally invariant and hence independent of the coordinate system, may be defined according to

$$\delta^* = \int_0^\infty \left\{ 1 - \frac{(u_1^2 + u_2^2)^{\frac{1}{2}}}{U_e} \right\} dx_3. \tag{4.17}$$

Using (3.2a) and the expansions in (3.23) and (3.25), it may be shown that

$$\delta^* = -\Delta_0 u_* \left\{ F_{1\infty} + u_* \left\{ F_{2\infty} + \frac{\beta_n^2}{2\gamma_0^2} S_{gg} \right\} + O(u_*^2) \right\}, \tag{4.18}$$

where the subscript '∞' denotes the evaluation of the quantity as $\eta \to \infty$ and

$$S_{gg} = \int_0^\infty G_1' G_1' \, \mathrm{d}\eta; \qquad (4.19)$$

in addition, $F_1(0) = F_2(0) = 0$ has been used. The outer-layer lengthscale Δ_0 may be defined as in two-dimensional boundary layers (Fendell 1972) according to

$$\Delta_0 = \delta^*/u_*, \qquad (4.20)$$

but where u_* is now given by (3.19). Then (4.18) implies that

$$F_{1\infty} = -1, \quad F_{2\infty} = -\frac{\beta_n^2}{2\gamma_0^2} S_{gg}. \qquad (4.21a, b)$$

A first integral of the first-order streamwise equation (4.11) may be easily obtained. Using the conditions

$$T_1 \to 1; \eta F_1', F_1 \to 0 \quad \text{as} \quad \eta \to 0, \quad T_1, \eta F_1' \to 0 \quad \text{as} \quad \eta \to \infty, \qquad (4.22a\text{–}e)$$

as well as (4.21 a), an integration of (4.11) from 0 to ∞ yields

$$\alpha_{s0} = 1 + \nu + 2\beta_s. \qquad (4.23)$$

Similarly, integration of the second-order streamwise equation (4.13) across the boundary layer gives

$$\alpha_{s1} = \frac{1+\nu+\beta_s}{\kappa} + (1+\beta_s) S_{ff} - \frac{\beta_n \alpha_{n0}}{\gamma_0} S_{fg} - \frac{\beta_n^2}{\gamma_0^2}(\tfrac{1}{2}+\beta_s-\nu) S_{gg}, \qquad (4.24)$$

where (4.21) has been used along with the following boundary conditions:

$$T_2, \eta F_2', F_2 \to 0 \quad \text{as} \quad \eta \to 0, \quad T_2, \eta F_2' \to 0 \quad \text{as} \quad \eta \to \infty. \qquad (4.25a\text{–}e)$$

The constants S_{ff} and S_{fg} appearing in (4.24) are defined as

$$S_{ff} = \int_0^\infty F_1' F_1' \, \mathrm{d}\eta, \quad S_{fg} = \int_0^\infty F_1' G_1' \, \mathrm{d}\eta, \qquad (4.26a, b)$$

which may be evaluated once the first-order equations (4.11) and (4.12) have been solved.

Next, define the positive quantity σ by

$$\sigma = \Delta_0 U_e/u_r. \qquad (4.27)$$

Upon differentiation and using (4.5) and (4.10), it is easily confirmed that

$$\partial\sigma/\partial x_1 = h_1 \alpha_{s0} + O(u_*), \quad \partial\sigma/\partial x_2 = h_2 \alpha_{n0} + O(u_*). \qquad (4.28a, b)$$

For a physically meaningful flow, σ must be a continuously differentiable function of (x_1, x_2) and consequently

$$\frac{\partial}{\partial x_2}(h_1 \alpha_{s0}) = \frac{\partial}{\partial x_1}(h_2 \alpha_{n0}). \qquad (4.29)$$

But from the definitions of K_1 and K_2 in (2.4) and using $h_1 = 1/U_e$, as well as (2.8), it follows that

$$K_1 = -\frac{1}{h_1 h_2}\frac{\partial h_2}{\partial x_1} = -\frac{\beta_s - \nu}{\sigma}, \quad K_2 = -\frac{1}{h_1 h_2}\frac{\partial h_1}{\partial x_2} = -\frac{\beta_n}{\sigma}. \qquad (4.30a, b)$$

Since α_{s0} and α_{n0} must be constant for a self-similar flow, it follows from (4.29) and (4.30) that

$$\alpha_{s0}\beta_n = \alpha_{n0}(\beta_s - \nu). \tag{4.31}$$

One further relation may be obtained by utilizing (3.3) and (3.4) to obtain

$$\frac{\partial U_e}{\partial x_1} = -\frac{U_e h_1}{\sigma}\beta_s, \quad \frac{\partial U_e}{\partial x_2} = -\frac{U_e h_2}{\sigma}\beta_n. \tag{4.32 a, b}$$

Since $U_e(x_1, x_2)$ must be continuously differentiable, it follows that

$$\frac{\partial}{\partial x_2}\left(\frac{U_e h_1 \beta_s}{\sigma}\right) = \frac{\partial}{\partial x_1}\left(\frac{U_e h_2 \beta_n}{\sigma}\right), \tag{4.33}$$

and using (4.28) and (4.30), it is easily shown that for β_s and β_n constant

$$\alpha_{n0}\beta_s = \beta_n(\alpha_{s0} + \nu). \tag{4.34}$$

Elimination of α_{n0} in (4.31) and (4.34) yields

$$\beta_n \nu(\alpha_{s0} + \nu - \beta_s) = 0. \tag{4.35}$$

Thus there are three possibilities for self-similarity. The first of these, corresponding to $\beta_n = 0$, is a degenerate case of flow without a cross-stream pressure gradient and will not be considered further. Consequently, there are only two cases to be addressed, (i) $\alpha_{s0} + \nu - \beta_s = 0$, and (ii) $\nu = 0$. Using (4.23) and (4.31), it can be shown that for case (i)

$$\nu = -\tfrac{1}{2}(1 + \beta_s), \quad \alpha_{s0} = \tfrac{1}{2}(1 + 3\beta_s), \quad \alpha_{n0} = \beta_n; \tag{4.36 a, b}$$

while for case (ii),

$$\nu = 0, \quad \alpha_{s0} = 1 + 2\beta_s, \quad \alpha_{n0} = (\beta_n/\beta_s)(1 + 2\beta_s). \tag{4.37 a, b}$$

The numerical procedure used to solve (4.11)–(4.14) also provides values for γ_0, γ_1, C_0 and C_1. Consequently, from (4.23), (4.36) or (4.37), all parameters are known except for β_s and β_n. Consequently, β_s and β_n form a two-parameter family of similarity solutions for three-dimensional turbulent boundary layers. There does not appear to be any reason to rule out case (i) or case (ii), and well-behaved solutions have been produced for both situations; however, for case (ii), β_s must be assumed to be $O(1)$. It is worthwhile to note that case (i) yields the same relationship for α_{s0} and ν as that obtained for plane-of-symmetry flow (Degani *et al.* 1992). The numerical results to be quoted in §7 are for case (i).

5. External flow leading to similarity

In this section it is demonstrated that self-similar boundary-layer flow can be achieved whenever the mainstream speed obeys a power-law distribution in distance along individual streamlines. For simplicity the following development is for case (i) solutions (equation (4.36)) although the results are similar to those obtainable for case (ii). Upon integration of (4.28 a) along a streamline (x_2 = constant), it follows that

$$\sigma = \tfrac{1}{2}(1 + 3\beta_s)(s - s_0), \tag{5.1}$$

where s denotes the distance along a streamline, and s_0 is the 'constant' of integration. From the definition (4.27), σ is always positive and therefore $s > s_0$ for $\beta_s > -\tfrac{1}{3}$ and $s < s_0$ for $\beta_s < -\tfrac{1}{3}$. Upon substitution of (5.1) into (4.32 a), it may be confirmed that

$$U_e = U_0 |s - s_0|^{-2\beta_s/(1 + 3\beta_s)}, \tag{5.2}$$

where $\beta_s \neq -\tfrac{1}{3}$ and U_0 is in general a function of x_2. The limiting case $\beta_s = -\tfrac{1}{3}$

(a) $\beta_s > -\frac{1}{3}$, $\beta_n < 0$ ($K_1 < 0$, $K_2 > 0$)   (b) $\beta_s > -\frac{1}{3}$, $\beta_n > 0$ ($K_1 < 0$, $K_2 < 0$)

(c) $\beta_s < -\frac{1}{3}$, $\beta_n < 0$ ($K_1 > 0$, $K_2 > 0$)   (d) $\beta_s < -\frac{1}{3}$, $\beta_n > 0$ ($K_1 > 0$, $K_2 < 0$)
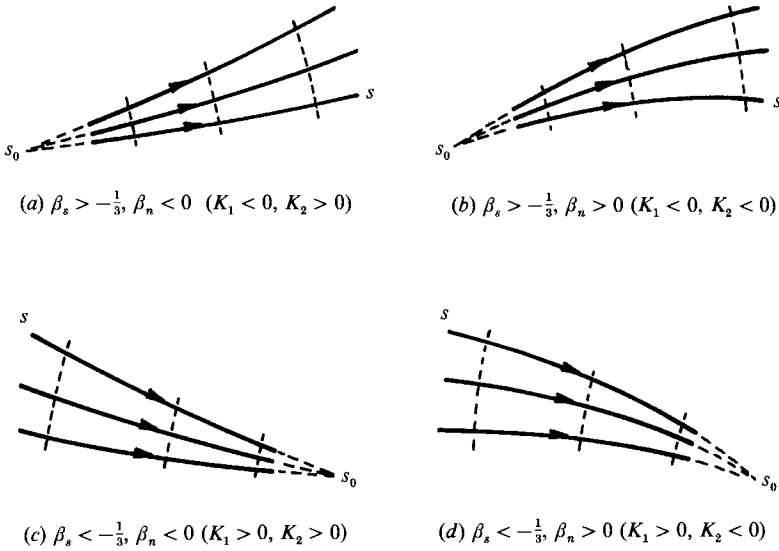
FIGURE 2. Typical external flow patterns that lead to self-similar boundary-layer flow.

corresponds to a highly accelerated flow in which σ is constant and $U_e \sim \exp(s)$; however, it can be shown (Degani 1991) that in this situation $K_1 = 0$ and K_2 is at most constant. Therefore, this limiting case degenerates to a two-dimensional or axisymmetric flow and will not be considered further.

Using (4.30), (4.36) and (5.1), the following results are obtained for the curvatures:

$$K_1 = -\frac{1}{s-s_0}, \quad K_2 = -\frac{2\beta_n}{1+3\beta_s}\frac{1}{s-s_0}, \quad \beta_s \neq -\tfrac{1}{3}. \qquad (5.3a, b)$$

With the definition of K_1 given by (2.4a), integration of (5.3a) yields the following expression for h_2:

$$h_2 = h_{20}|s-s_0|, \qquad (5.4)$$

where h_{20} is, in general, a positive function of x_2. The function h_{20} is not arbitrary in general; a relation connecting U_0 and h_{20} has been derived in Degani (1991) but is not needed for the discussion to follow here.

In figure 2, some typical external flow patterns leading to similarity in the boundary layer are sketched. In the situations shown in figures 2(a) and 2(b), the external streamlines diverge from each other in the flow direction so that h_2 increases with $\beta_s > -\frac{1}{3}$ and $s > s_0$. The velocity distribution along a streamline is given by (5.2). Furthermore, from (5.3a), it follows that $K_1 < 0$. Since $\beta_s > -\frac{1}{3}$, the flow patterns depicted in figures 2(a) and 2(b) may be achieved with either a favourable $(-\frac{1}{3} < \beta_s < 0)$ or an adverse $(\beta_s > 0)$ streamwise pressure gradient and the resulting similarity solutions are realized for $(s-s_0)$ large and positive. On the other hand, for the situations shown in figures 2(c) and 2(d) the external streamlines converge in the direction of the flow with h_2 decreasing with increasing s. In both cases, $\beta_s < -\frac{1}{3}$; hence, such flows are realized for favourable streamwise pressure gradients only.

For the cases shown in figures 2(a) and 2(c), the streamlines are concave up $(K_2 > 0)$, while in figures 2(b) and 2(d) the streamlines are concave down $(K_2 < 0)$. In all cases, the velocity profile skews in the direction towards the centre of curvature of the external streamlines. Consequently, for the flows in figures 2(a) and 2(c), the skew angle at the wall $\theta_w > 0$, and, for the flows in figures 2(b) and 2(d), $\theta_w < 0$; hence, the

sign of K_2 and θ_w is the same. Since u_* and σ are always positive, it follows from (3.21) that θ_* and θ_w are of the same sign and from (4.30b), K_2 and β_n are of opposite sign. Therefore, for self-similar flow, it follows from (3.36) that the parameter γ is always positive.

In general, γ may become negative under special circumstances, and in this context it is of interest to discuss the situation when the cross-stream velocity develops an S-shaped profile. Consider the cross-stream profile depicted schematically in figure 1 and assume that at some location downstream the external streamline changes curvature so that the cross-stream pressure gradient changes from positive to negative. The inertia of the fluid in the wall layer is much smaller than in the outer layer and hence the near-wall flow will respond quickly, but not immediately, by eventually skewing in the positive x_2-direction. Consequently, for a relatively short streamwise distance, K_2 and θ_w are of opposite sign and therefore $\gamma < 0$. Once the wall-layer flow skews in the positive x_2-direction, then $\gamma > 0$ once again. On the other hand, the fluid in the outer layer is slower to respond to the change in cross-stream pressure gradient and a zone of flow in the negative x_2-direction persists in the outer layer, thus giving rise to an S-shaped profile. Eventually, of course, the cross-stream flow will all be in the positive x_2-direction, provided that the curvature of the external streamline does not change again. For the similarity solutions considered here, it is evident from (5.3b) that K_2 cannot change sign; consequently, self-similar S-shaped profiles do not appear to be possible.

6. Turbulence closure and similarity solutions

Although the results in §3 were obtained without any turbulence-closure assumption, a specific model must be adopted in order to solve the similarity equations (4.11)–(4.16). The main intent here is to construct similarity solutions using a simple self-consistent model to illustrate the dependence of the velocity and shear stress profiles on Reynolds number and pressure gradient. It is worthwhile to stress that no attempt will be made here to try to infer a 'best turbulence model' through direct comparison with experimental data. Consequently a simple representative algebraic model is used here which is defined by

$$\tau_{13} = \epsilon_1 \, \partial u_1 / \partial x_3, \quad \tau_{23} = \epsilon_2 \, \partial u_2 / \partial x_3, \quad (6.1\,a,\,b)$$

where ϵ_1 and ϵ_2 are the total (turbulent + kinematic) viscosities in the streamwise and cross-stream directions, respectively. In principle, ϵ_1 could have a representation in terms of an expansion in powers of u_*. However, if ϵ_1 is taken to be represented by one term (Degani *et al.* 1992), then substitution of the expansions (3.25) and (3.32) for the streamwise velocity and total shear stress, respectively, into (6.1a) and using (4.20) yields

$$T_1 = \frac{\epsilon_1}{U_e \, \delta^* \sec \theta_w} \frac{\partial^2 F_1}{\partial \eta^2}, \quad T_2 = \frac{\epsilon_1}{U_e \, \delta^* \sec \theta_w} \frac{\partial^2 F_2}{\partial \eta^2}. \quad (6.2\,a,\,b)$$

From (3.17) and (3.33), (6.2a) implies that

$$\epsilon_1 \sim U_e \, \delta^* \sec \theta_w \, \kappa \eta + \dots \quad \text{as} \quad \eta \to 0. \quad (6.3)$$

Similarly, if ϵ_2 is also assumed to be represented by a single term, it follows from (3.23) and (3.34) that

$$\tilde{T}_1 = \frac{\epsilon_2}{U_e \, \delta^* \sec \theta_w} \frac{\partial^2 G_1}{\partial \eta^2}, \quad \tilde{T}_2 = \frac{\epsilon_2}{U_e \, \delta^* \sec \theta_w} \frac{\partial^2 G_2}{\partial \eta^2}. \quad (6.4\,a,\,b)$$

From (3.24b), (3.35), and (6.4), it follows that ϵ_2 must also satisfy (6.3) and thus both components of the total viscosity are equal in the limit as $\eta \to 0$, to leading order. A simple model satisfying the required asymptotic behaviour is

$$\epsilon_1 = \epsilon_2 = U_e \delta^* \epsilon_m, \qquad (6.5)$$

where
$$\epsilon_m = \begin{cases} K, & \eta \geqslant K/\kappa, \\ \kappa\eta, & \eta < K/\kappa, \end{cases} \qquad (6.6)$$

since, from (3.21), $\sec\theta_w \sim 1 + O(u_*^2)$. Here κ is the von Kármán constant and K is a constant assumed to be 0.016 (Mellor & Gibson 1966). The model captures the essence of a class of algebraic turbulence models (Mellor & Gibson 1966; Cebeci & Smith 1975; Baldwin & Lomax 1978) for the outer layer; so-called outer-layer 'intermittency' corrections are omitted here since they have little influence on evaluation of the velocity profile. It may be noted that since (6.5) and (6.6) are only used in the outer layer, a wall-layer damping function is not required. Several experimental data sets indicate that the inferred ratio of eddy viscosities ϵ_2/ϵ_1 is not unity in the outer layer (see, for example, Bradshaw & Pontikos 1985; Anderson & Eaton 1989). A non-isotropic model could be introduced in the present formulation in at least two ways. First higher-order non-isotropic terms could be introduced in (6.5), although at present there does not appear to be a fundamental basis for selecting such models. Second a non-isotropic outer-layer model may be introduced in (6.5) by adopting a different value of the constant K in each coordinate direction (Degani *et al.* 1992). Such models have been considered but do not have a significant influence on the general features of the velocity profiles to be described in §7 nor on the evaluation of the wall shear stress. Thus the model (6.5) may be regarded as the simplest possible turbulence model, representative of modern algebraic three-dimensional models (see, for example, Wie & DeJarnette 1988).

Substitution of (4.36) and the turbulence model (6.3)–(6.6) into the first-order equations (4.11) and (4.12) gives

$$(\epsilon_m F_1'')' + (1+2\beta_s)\,\eta F_1'' + 2\beta_s F_1' = 0, \qquad (6.7)$$

$$(\epsilon_m G_1'')' + (1+2\beta_s)\,\eta G_1'' - \tfrac{1}{2}(1+\beta_s)\,G_1' = 2\gamma_0 F_1', \qquad (6.8)$$

with the boundary conditions

$$F_1' \to \frac{1}{\kappa}\log\eta + C_0, \quad G_1' \sim 1 \quad \text{as} \quad \eta \to 0, \qquad (6.9a,b)$$

$$F_1', G_1' \to 0 \quad \text{as} \quad \eta \to \infty. \qquad (6.9c,d)$$

It may be confirmed that the second-order equations are given by

$$(\epsilon_m F_2'')' + (1+2\beta_s)\,\eta F_2'' + 2\beta_s F_2' = Z_1, \qquad (6.10)$$

$$(\epsilon_m G_2'')' + (1+2\beta_s)\,\eta G_2'' - \tfrac{1}{2}(1+\beta_s)\,G_2' = Z_2, \qquad (6.11)$$

where

$$Z_1(\eta) = -\frac{1+\beta_s}{2\kappa}F_1' - \alpha_{s1}\,\eta F_1'' - (1+2\beta_s)\,F_1 F_1'' - \beta_s(F_1')^2 + \frac{\beta_n^2}{\gamma_0}G_1 F_1'' - \frac{(1+3\beta_s)\,\beta_n^2}{2\gamma_0^2}(G_1')^2, \qquad (6.12)$$

$$Z_2(\eta) = 2\gamma_0 F_2' + 2\gamma_1 F_1' - \frac{1+\beta_s}{2\kappa}G_1' - \alpha_{s1}\,\eta G_1'' + \frac{1+\beta_s}{2}F_1' G_1'$$

$$-(1+2\beta_s)\,F_1 G_1'' + \frac{\beta_n^2}{\gamma_0}(G_1')^2 + \frac{\beta_n^2}{\gamma_0}G_1 G_1'' + \gamma_0(F_1')^2, \qquad (6.13)$$

with α_{s1} given by (4.24). The boundary conditions are

$$F_2' \sim C_1, \quad G_2' \sim (1/\kappa) \log \eta + C_0, \quad \text{as} \quad \eta \to 0, \qquad (6.14a, b)$$

$$F_2', G_2' \to 0 \quad \text{as} \quad \eta \to \infty. \qquad (6.14c, d)$$

Note that, for case (i), the similarity equations (6.7)–(6.14) are identical to those obtained for the flow near a plane of symmetry (Degani *et al.* 1992) except for some differences in the form of the forcing functions Z_1 and Z_2. A numerical procedure to obtain an accurate solution of these equations is described in the Appendix and in greater detail by Degani (1991). It is a two-tier scheme utilizing a series expansion for small η and a finite-difference solution for larger values of η. For a given value of β_s, the constants C_0 and γ_0 are obtained as part of the numerical solution of (6.7) and (6.8). Once F_1 and G_1 are known, the constants in (4.19), (4.24) and (4.26) are calculated, and for a given β_n, all constants appearing in (6.10)–(6.14) are known. Finally, the constants C_1 and γ_1 are obtained as part of the solution of (6.10) and (6.11). Consequently, the second-order contribution to θ_* may be determined from (4.9).

A Reynolds number based on the lengthscale δ^* (cf. (4.17)) may be defined by $Re_{\delta*} = Re \, U_e \delta^*$, and (3.27) becomes

$$\frac{1}{u_*} = \frac{1}{\kappa} \log Re_{\delta*} + C_i - C_0 - u_* C_1 + \dots. \qquad (6.15)$$

With C_0 and C_1 calculated, (6.15) provides an equation to determine the scaled friction velocity u_* in terms of a given $Re_{\delta*}$; note that a first-order estimate for u_* is obtained by equating C_1 to zero in (6.15). Finally, the skew angle θ_w and friction velocity are determined from

$$\theta_w = \tan^{-1}\{u_* \theta_*\}, \quad u_\tau / U_e = u_* \sec \theta_w. \qquad (6.16a, b)$$

7. Results and discussion

The calculated solutions of the similarity equations show that the second-order corrections to u_* and the outer-layer streamwise profiles are small at the large Reynolds numbers considered in this study and for all practical purposes may be neglected. Consequently, from (3.16) and (3.22c), a composite streamwise velocity profile is

$$u_1 / U_e = \{1 + u_* \, dF_1/d\eta\} + u_* U^+ - U_c, \qquad (7.1)$$

where U_c is the common contribution, written in terms of the wall-layer variable by

$$U_c = u_*\{(1/\kappa) \log y^+ + C_i\}. \qquad (7.2)$$

In contrast, both terms in (3.23) are necessary to describe the cross-stream velocity profile in the outer layer (see also Degani *et al.* 1992). Using (3.22d), a composite profile is

$$\frac{u_2}{U_e \tan \theta_w} = \left\{\frac{dG_1}{d\eta} + u_* \frac{dG_2}{d\eta}\right\} + u_* U^+ - U_c, \qquad (7.3)$$

where (3.21) has been used to define an appropriate non-dimensionalizing quantity for u_2. The wall-layer velocity profile U^+ given by Walker *et al.* (1989) was used to define the composite profiles.

Similarity solutions for the full three-dimensional flow were calculated for a variety of cases. The results presented here are for the conditions

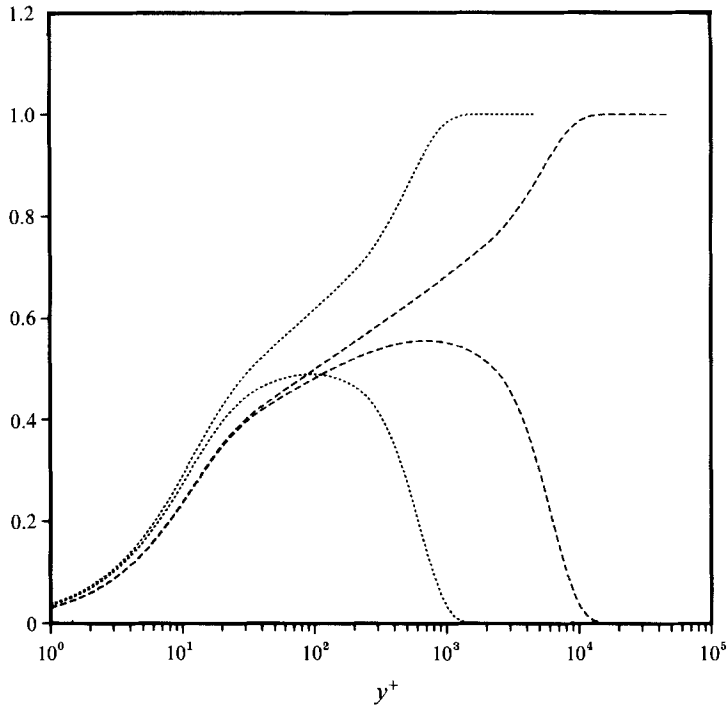$$\beta_s = 0.5, \quad \beta_n = -0.2, \qquad (7.4a, b)$$

FIGURE 3. The streamwise and cross-stream velocity profiles for $\beta_s = 0.5$ and $\beta_n = -0.2$:
$\cdots\cdots$, $Re_{\delta*} = 5000$; ————, $Re_{\delta*} = 50000$.

and are representative of the other situations considered. The four constants obtained as part of the numerical solution are (to three significant figures)

$$C_0 = -1.29, \quad \gamma_0 = 0.124; \quad C_1 = 0.394, \quad \gamma_1 = -0.665. \qquad (7.5\,a-d)$$

Note that the scaled wall skew angle at the wall may be evaluated from (4.9) using this information.

The streamwise and cross-stream velocity profiles for two values of the Reynolds number, namely $Re_{\delta*} = 5000$ ($u_* = 0.0369$) and $Re_{\delta*} = 50000$ ($u_* = 0.0306$), with the pressure-gradient parameters given by (7.4), are plotted in figure 3; here the quoted value of u_* is the first-order estimate obtained from (6.15) with $C_1 = 0$. Although both profiles contain a logarithmic variation in the overlap region, figure 3 indicates that this behaviour is not evident at the lower Reynolds number. However, at the higher value of the Reynolds number, the logarithmic variation is well-defined for both velocity components. Another noteworthy feature of the result in figure 3 is the extent of near-wall collateral flow. At $Re_{\delta*} = 5000$, the two profiles coincide to only $y^+ = 5$, but at $Re_{\delta*} = 50000$, the profiles coincide to about $y^+ = 50$, indicating that the extent of collateral flow in terms of the wall-layer variable increases with increasing Reynolds number. The results in figure 3 perhaps also explain why the issue of the extent of near-wall collateral flow is controversial in the literature, and why the logarithmic nature of the cross-stream velocity has not been observed in experimental data obtained at relatively lower Reynolds numbers.

Next, the effect of Reynolds number on the cross-stream velocity profile is considered. The composite profiles for the cross-stream velocity given by (7.3) are plotted in figure 4 for various Reynolds numbers for the values of the pressure-gradient
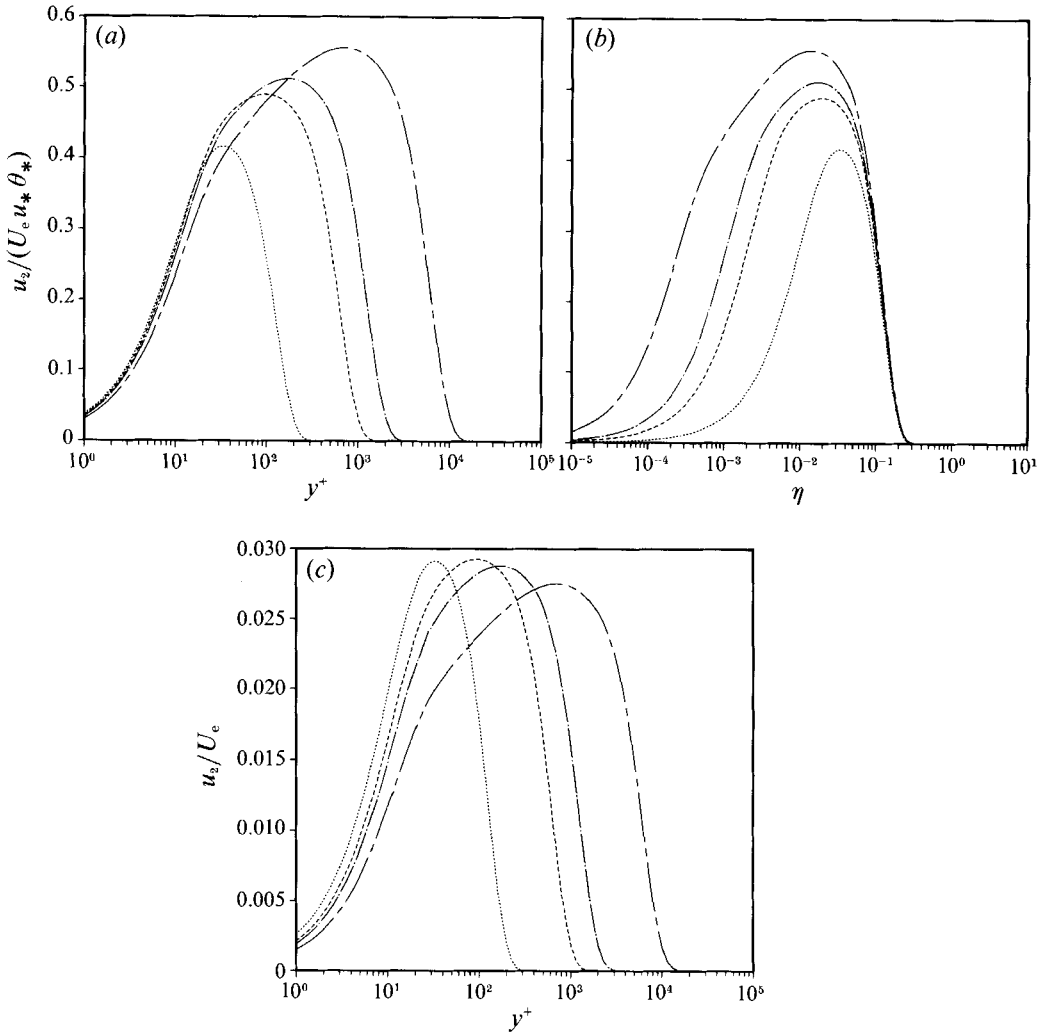
FIGURE 4. Cross-stream velocity profiles for $\beta_s = 0.5$ and $\beta_n = -0.2$: $\cdots\cdots$, $Re_{\delta*} = 1000$; ————, $Re_{\delta*} = 5000$; —·—·—, $Re_{\delta*} = 10000$; —————, $Re_{\delta*} = 50000$. (a) In terms of the wall-layer variable y^+. (b) In terms of the outer-layer variable η. (c) In terms of the normalization in (7.15).

parameters listed in (7.4). These profiles are plotted in terms of the wall-layer variable y^+ in figure 4(a) and the outer variable in figure 4(b). Although the composite profile for u_2 contains a logarithmic variation in the overlap zone, the logarithmic portion of the profile is clearly evident in figures 4(a) and 4(b) only at the highest Reynolds number. In terms of y^+, the location of the maximum, say y^+_{max}, becomes substantially larger with increasing $Re_{\delta*}$ as shown in figure 4(a). On the other hand, in terms of the outer variable, the location of the maximum denoted by η_{max} decreases slightly with increasing $Re_{\delta*}$ as indicated in figure 4(b). To explain this behaviour in u_2, consider the cross-stream total stress function τ_{23} defined in (3.34). It follows from (3.35) that

$$\frac{\tau_{23}}{u_\tau^2 \cos\theta_w \theta_*} \sim \frac{2\gamma}{\kappa}\eta\log\eta + \ldots + u_*\left\{1 + \frac{\gamma}{\kappa^2}\eta\log^2\eta + \ldots\right\} \quad \text{as} \quad \eta \to 0, \qquad (7.6)$$

which is a result that is independent of a specific turbulence model. However, for the model adopted in (6.4), the maximum in cross-stream velocity occurs at the point

where τ_{23} is zero. It will now be shown that this maximum occurs within the overlap zone. Define an intermediate variable $\xi = x_3/\varDelta_m$ such that $\varDelta_i/\varDelta_m$, $\varDelta_m/\varDelta_o \to 0$ as $Re \to \infty$. The scale $\varDelta_m$ is to be determined by requiring that $\xi \sim O(1)$ where $\tau_{23} = 0$. For convenience, let $\varDelta_m = \chi\varDelta_o$, where χ is to be found subject to the requirement that $\chi \to 0$ as $Re \to \infty$. Writing (7.6) in terms of the intermediate variable ξ and isolating the dominant behaviour as $\chi \to 0$ with ξ fixed leads to

$$\frac{\tau_{23}}{u_\tau^2 \cos\theta_w\,\theta_*} \sim \frac{2\gamma}{\kappa}\xi\chi\log\chi + u_* + \dots \quad \text{as} \quad Re \to \infty. \tag{7.7}$$

Consequently, the location of the maximum cross-stream velocity in terms of ξ may be written as $\xi_{max} = \kappa/(2\gamma)$, where χ is given by the equation

This relation gives
$$-\chi\log\chi = u_*. \tag{7.8}$$

$$\chi \sim \frac{u_*}{-\log u_*}\left\{1 + \frac{\log(-\log u_*)}{\log u_*} + \dots\right\} \quad \text{as} \quad u_* \to 0. \tag{7.9}$$

This scaling of χ establishes the result that the maximum in cross-stream velocity is located within the overlap zone.

The location of the maximum cross-stream velocity may also be expressed in terms of the outer-layer variable η. Retaining only the leading-order term in (7.9) leads to

$$\eta_{max} = \frac{\kappa u_*}{2\gamma(-\log u_*)}. \tag{7.10}$$

It follows from (6.15) that u_* is $O(1/\log Re_{\delta^*})$ as $Re_{\delta^*} \to \infty$ and thus

$$\eta_{max} = O\left(\frac{1}{\log Re_{\delta^*}\log(\log Re_{\delta^*})}\right) \quad \text{as} \quad Re_{\delta^*} \to \infty. \tag{7.11}$$

This confirms the slow decrease in η_{max} with increasing Re_{δ^*} that may be observed in figure 4(b). On the other hand, in terms of the inner variable,

$$y^+_{max} = \eta_{max}Re_{\delta^*}, \tag{7.12}$$

and it follows that y^+_{max} must increase rapidly with Re_{δ^*}, as seen in figure 4(a).

Another noteworthy feature in figures 4(a) and 4(b) is the increasing value of the maximum cross-stream velocity with increasing Re_{δ^*}. It follows from (3.23) and (3.24) that

$$\frac{u_2}{U_e\tan\theta_w} \sim 1 + \dots + u_*\left\{\frac{1}{\kappa}\log\eta + C_0\right\} + \dots \quad \text{as} \quad \eta \to 0. \tag{7.13}$$

Writing this equation in terms of the intermediate variable and using the leading-order result in (7.9) it can be shown that

$$\frac{u_2}{U_e\tan\theta_w} \sim 1 + \frac{u_*}{\kappa}\log u_* + \dots \quad \text{as} \quad \eta \to \eta_{max}. \tag{7.14}$$

The second term on the right-hand side of (7.14) is negative and, consequently, the maximum value of $u_2/(U_e\tan\theta_w)$ increases towards 1 as $Re_{\delta^*} \to \infty$. However, the maximum value of u_2 itself is expected to decrease with increasing Re_{δ^*} and to illustrate this, it is useful to consider an alternative normalization for the cross-stream velocity function that does not involve the Reynolds number. Substituting (3.21) and the leading term in (4.9) into (7.3) results in

$$\frac{u_2}{U_e} = -\frac{\beta_n}{\gamma_0}u_*\left\{\left\{\frac{\partial G_1}{\partial\eta} + u_*\frac{\partial G_2}{\partial\eta}\right\} + u_*\,U^+ - U_c\right\}, \tag{7.15}$$
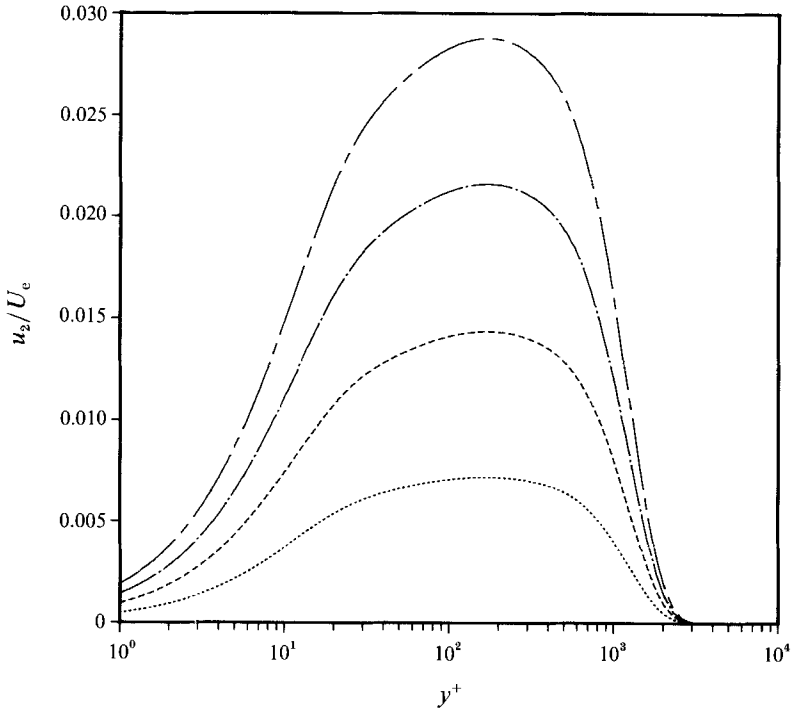
FIGURE 5. Effect of the cross-stream pressure gradient on the cross-stream velocity profile for $\beta_s = 0.5$ and $Re_{\delta*} = 10000$: $\cdots\cdots$, $\beta_n = -0.05$; $----$, $\beta_n = -0.1$; $-\cdot-\cdot-$, $\beta_n = -0.15$; $-\cdot\cdot-\cdot\cdot-$, $\beta_n = -0.2$.

Profile	β_n	C_1	γ_1
2	-0.05	0.578	-0.663
2	-0.10	0.541	-0.663
3	-0.15	0.480	-0.664
4	-0.20	0.394	-0.665

TABLE 1. Values of the parameters for four calculated profiles

where only the leading term in the expansion (4.8) for γ has been retained. The profile function (7.15) is representative of the actual cross-stream velocity attained in physical space; it is plotted in figure 4(c) where it may be noted that the maximum value of cross-stream velocity decreases as $Re_{\delta*} \to \infty$.

In order to illustrate the influence of the cross-stream pressure gradient on the cross-stream velocity profile, the Reynolds number was arbitrarily fixed at $Re_{\delta*} = 10000$ and the outer-layer similarity solution was computed for three additional values of the cross-stream pressure-gradient parameter β_n with β_s held fixed at 0.5. The parameters computed from the numerical solutions are given in table 1; for each case, γ_0 and C_0 are given by (7.5a, b). The normalized cross-stream profile given by (7.15) yields the most representative picture of the actual cross-stream velocity distribution and is plotted in figure 5. The scaled wall skew angle may be evaluated from (6.16), and both it and the cross-stream velocity increase with increasing cross-stream gradient as expected.
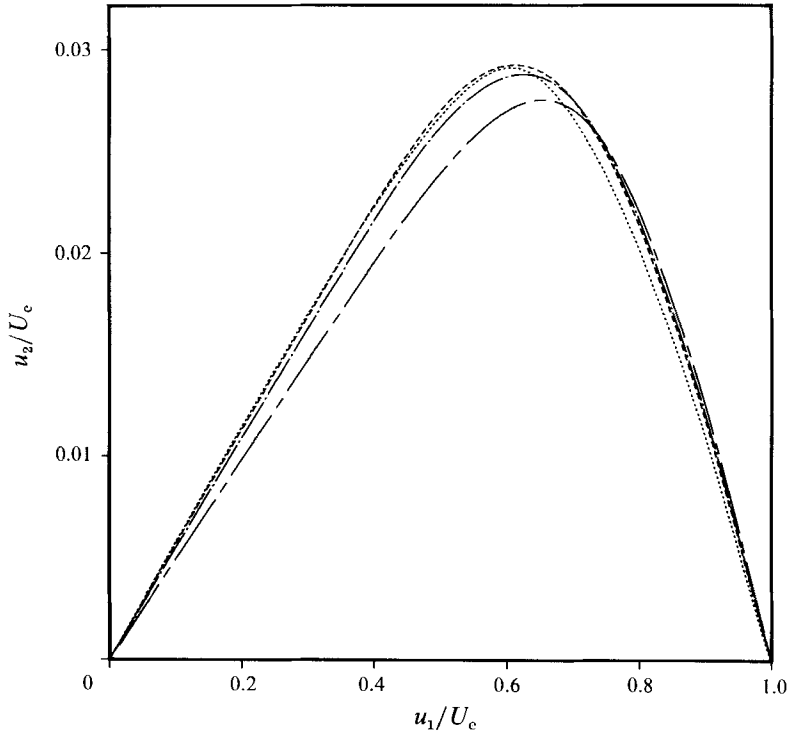
FIGURE 6. Hodograph plot of the cross-stream velocity with respect to the streamwise velocity for $\beta_s = 0.5$ and $\beta_n = -0.2$: $\cdots\cdots$, $Re_{\delta^*} = 1000$; $----$, $Re_{\delta^*} = 5000$; $-\cdot-\cdot-$, $Re_{\delta^*} = 10000$; $-----$, $Re_{\delta^*} = 50000$.

It is common practice in the literature (for example, Johnston 1960; Hornung & Joubert 1963; Goldberg & Reshotko 1984) to present the streamwise and cross-stream velocities in terms of a hodograph plot and, following this tradition, the results in figures 3 and 4 are replotted in figure 6 in this format. The normalization in (7.15) is used for the cross-stream velocity profile. Plots of this nature are the basis of the empirical 'triangle law' which appears to be a reasonable approximation over a range of Reynolds numbers; note, however, that since $\theta_w \to 0$ as $Re \to \infty$, the slope of the left side of the triangle decreases with increasing Reynolds number. It is of interest to note that the structural details of the cross-stream velocity profile, apparent in figures 3 and 4, are disguised when plotted in the hodograph form in figure 6.

8. Conclusions

The asymptotic structure of the three-dimensional turbulent boundary layer in the limit of large Reynolds number has been derived. The streamwise velocity profile is similar to that in two-dimensional boundary layers with a defect-function form in the outer layer; however, the velocity scale of the defect includes a dependence on the wall skew angle. The leading-order term in the outer-layer expansion of the cross-stream velocity profile asymptotes to a constant but the second-order term behaves logarithmically as the wall layer is approached. It was shown that the characteristic 'bulge' in the cross-stream velocity is a natural consequence of the asymptotic structure, and that the wall skew angle scales on the friction velocity. Although the flow

in the wall layer is collateral to leading order, the higher-order effects of the pressure gradient are not negligible at the large but finite Reynolds numbers in practice and can cause the profiles in the wall layer to skew substantially.

Conditions that must be satisfied by the external flow in order for the boundary layer to achieve self-similarity were derived. It was determined that the streamwise and cross-stream pressure-gradient parameters form a two-parameter family of similarity solutions. By using a simple turbulence-closure model consistent with the results of the asymptotic analysis, similarity solutions for the outer layer were obtained which were then matched asymptotically to an analytical wall-layer profile. The composite solution so obtained described the velocity profiles throughout the thickness of the boundary layer. It was shown that the extent of collateral flow in the near-wall region, measured in terms of the wall variable y^+, increased with increasing Reynolds number. Furthermore, a logarithmic profile for the cross-stream velocity was not apparent at low Reynolds numbers, but became clearly defined at higher values.

The effects of Reynolds number and cross-stream pressure gradient on the cross-stream velocity profile were investigated. It was demonstrated that, with increasing Reynolds number, the location of the maximum cross-stream velocity from the wall increased in terms of the wall variable y^+, but decreased in terms of the outer variable η. It was determined that the location of the maximum cross-stream velocity is neither in the outer nor wall layers, but within the overlap region between the two layers. It was shown that the magnitude of the maximum cross-stream velocity increased with decreasing Reynolds number and increasing cross-stream pressure gradient.

Finally, it must be noted that the present theory pertains to an attached turbulent boundary layer; it is not expected to be applicable to a flow approaching separation where very large wall skew angles have been observed experimentally. The structure of the near-wall flow presented here is generally consistent with the dynamical model of time-dependent turbulent flow near a wall as discussed by Smith *et al.* (1991). On the other hand, the dynamics of the instantaneous flow in the region of a separating boundary layer are complex and poorly understood; consequently, it is expected that the structure in such regions is more complex than the two-layer structure considered here.

Appendix

The numerical algorithm to solve (6.7)–(6.14) is a two-tiered procedure (Walker & Stewartson 1974; Yuhas & Walker 1982), using a series expansion for small η in the inner tier and a numerical solution for $\eta > \eta_m$ in the outer tier. Here η_m denotes the boundary between the two tiers where the two solutions are joined smoothly together; here $\eta_m < K/\kappa$, but the results are independent of the specific values used.

First, consider the inner tier where the solution of either (6.7) or (6.8) is of the form (Degani 1991)

$$\mathscr{L}_1 = \sum_{n=0}^{\infty} a_n \eta^n + \log \eta \sum_{n=0}^{\infty} b_n \eta^n. \tag{A 1}$$

Recursion relations for the coefficients a_n and b_n are readily obtained by substituting (A 1) into (6.7) and (6.8) and using (6.9 a, b). The solution of either of the second-order equations (6.10) or (6.11) has the general form

$$\mathscr{L}_2 = \sum_{n=0}^{\infty} s_n \eta^n + \log \eta \sum_{n=0}^{\infty} t_n \eta^n + log^2 \eta \sum_{n=1}^{\infty} u_n \eta^n, \tag{A 2}$$

and formulae for the coefficients s_n, t_n and u_n may be obtained upon substituting (A 2) into (6.10) and (6.11). However, the expressions for the coefficients are long and are given elsewhere (Degani 1991).

Consider the first-order streamwise equation (6.7) and for convenience $F_1'(\eta)$ is denoted by f. With β_s specified, the constant C_0 in condition (6.9a) is to be found. If two arbitrary values of the constant C_0, denoted by C_0^1 and C_0^2 are assumed, two series solutions in the inner tier, denoted by f_s^1 and f_s^2, are obtained. Each series evaluated at η_m provides a boundary condition which may be used to obtain numerical solutions (denoted f_n^1 and f_n^2) in the outer tier $\eta_m < \eta < \infty$, using standard boundary-value procedures. Since (6.7) is linear, a linear combination of the two solutions is also a solution; hence

$$f_s = B_1 f_s^1 + B_2 f_s^2, \quad f_n = B_1 f_n^1 + B_2 f_n^2, \tag{A 3a, b}$$

in the inner and outer tier, respectively. Here B_1 and B_2 are constants with

$$B_1 + B_2 = 1, \quad B_1 C_0^1 + B_2 C_0^2 = C_0, \tag{A 4a, b}$$

in order to satisfy (6.9a). To ensure a continuous first derivative at η_m, it follows from (A 3) that

$$B_1(f_n^{1\prime} - f_s^{1\prime}) + B_2(f_n^{2\prime} - f_s^{2\prime}) = 0 \quad \text{at} \quad \eta = \eta_m, \tag{A 5}$$

where the primes denote differentiation with respect to η. The slope of the series solution is obtained analytically from (A 1), and for the numerical solution a six-point forward-difference formula is used (Abramowitz & Stegun 1965). The constants B_1, B_2, and C_0 are evaluated from (A 4) and (A 5) and the true solution is then constructed from (A 3).

For the first order cross-stream equation (6.8), the constant γ_0 is unknown. Using a similar approach, a solution for $G_1'(\eta)$ may be constructed by assuming two arbitrary values of γ_0 to generate series solutions in the inner tier and numerical solutions in the outer tier. A linear combination of these two solutions is then obtained which satisfies (6.9b) and has a continuous first derivative at $\eta = \eta_m$. In this manner, γ_0 and the true solution for $G_1'(\eta)$ is produced. For the second-order problems, consider the forcing functions in (6.12) and (6.13). From the known first-order solutions, the constants S_{ff}, S_{fg}, S_{gg} defined in (4.19) and (4.26) are obtained and used to calculate α_{s1} from (4.24). In this manner, only two unknown constants remain in the second-order equations, namely C_1 and γ_1. Since the form of the second-order equations is similar to that of the first-order equations, they may be solved in the same manner to yield the second-order solutions $F_2'(\eta)$ and $G_2'(\eta)$ along with the correct values of C_1 and γ_1.

In the above procedure, it is necessary to evaluate the derivatives in the outer tier numerically. Since η_m is small and the solutions contain logarithmic behaviour for small η, significant error may be incurred in the evaluation of the relatively large gradients and, hence, B_1 and B_2. By introducing the transformation $\xi = \log \eta$ in the outer tier, it follows from (6.9a) that

$$\mathrm{d}f/\mathrm{d}\xi \to 1/\kappa \quad \text{as} \quad \xi \to -\infty. \tag{A 6}$$

The slope is $O(1)$ in the transformed systems and this facilitates the accurate evaluation of B_1 and B_2. A uniform mesh in ξ is used, and this produces a fine mesh near the wall in terms of η, with a relatively coarse mesh farther away.

REFERENCES

ABRAMOWITZ, M. & STEGUN, I. 1965 *Handbook of Mathematical Functions*. Dover.

ANDERSON, S. D. & EATON, J. K. 1989 Reynolds stress development in pressure-driven three-dimensional turbulent boundary layers. *J. Fluid Mech.* **202**, 263–294.

BALDWIN, B. S. & LOMAX, H. 1978 Thin layer approximation and algebraic model for separated turbulent flows. *AIAA Paper* 78-257, *16th Aerosciences Meeting, Huntsville, Alabama, January 16–18.*

BARNWELL, R. W., WAHLS, R. A. & DEJARNETTE, F. E. 1988 A defect stream function, law of the wall/wake method for turbulent boundary layers. *AIAA Paper* 88-0127, *26th Aerospace Sciences Meeting, Reno, Nevada.*

BRADSHAW, P. & PONTIKOS, N. S. 1985 Measurements in the turbulent boundary layer on an 'infinite' swept wing. *J. Fluid Mech.* **159**, 105–130.

CEBECI, T. & SMITH, A. M. O. 1974 *Analysis of Turbulent Boundary Layers*. Academic.

CLAUSER, F. H. 1954 Turbulent boundary layers in adverse pressure gradients. *J. Aeronaut. Sci.* **21**, 91–108.

CLAUSER, F. H. 1956 The turbulent boundary layer. *Adv. Appl. Mech.* **4**, 1–51.

DEGANI, A. T. 1991 The three-dimensional turbulent boundary layer – theory and application. Ph.D. thesis, Lehigh University.

DEGANI, A. T., SMITH, F. T. & WALKER, J. D. A. 1992 The three-dimensional turbulent boundary layer near a plane of symmetry. *J. Fluid Mech.* **234**, 329–360.

DEGANI, A. T. & WALKER, J. D. A. 1991 Computation of three-dimensional turbulent boundary layers using the embedded-function method. *AIAA Paper* 92-0440, *30th Aerospace Sciences Meeting, Reno, Nevada, January 6–9.*

FENDELL, F. E. 1972 Singular perturbation and turbulent shear flow near walls. *J. Astro. Sci.* **20**, 129–165.

FERNHOLZ, H. H. & VAGT, J.-D. 1981 Turbulence measurements in an adverse-pressure-gradient three-dimensional turbulent boundary layer along a circular cylinder. *J. Fluid Mech.* **111**, 233–269.

GOLDBERG, U. & RESHOTKO, E. 1984 Scaling and modeling of three-dimensional pressure-driven turbulent boundary layers. *AIAA J.* **22**, 914–920.

HORNUNG, H. G. & JOUBERT, P. N. 1963 The mean velocity profile in three-dimensional turbulent boundary layers. *J. Fluid Mech.* **15**, 368–384.

JOHNSTON, J. P. 1960 On three-dimensional turbulent boundary layers generated by secondary flow. *Trans. ASME* D: *J. Basic Engng* **82**, 233–246.

MELLOR, G. L. 1972 The large Reynolds number, asymptotic theory of turbulent boundary layers. *Intl J. Engng Sci.* **10**, 851–873.

MELLOR, G. L. & GIBSON, D. M. 1966 Equilibrium turbulent boundary layers. *J. Fluid Mech.* **24**, 225–253.

NASH, J. F. & PATEL, V. C. 1972 *Three-Dimensional Turbulent Boundary Layers*. Atlanta: SBC Technical Book.

PIERCE, F. J., MCALLISTER, J. E. & TENNANT, M. H. 1983 A review of near-wall similarity models in three-dimensional turbulent boundary layers. *Trans. ASME* I: *J. Fluids Engng* **105**, 251–262.

PIERCE, F. J. & ZIMMERMAN, B. B. 1973 Wall shear stress inference from two- and three-dimensional turbulent boundary layer velocity profiles. *Trans. ASME* I: *J. Fluids Engng* **95**, 61–67.

PRAHLAD, T. S. 1973 Mean velocity profiles in three-dimensional incompressible turbulent boundary layers. *AIAA J.* **11**, 359–365.

RUBESIN, M. R. & VIEGAS, J. R. 1985 A critical examination of the use of wall functions as boundary conditions in aerodynamic calculations. *Third Symp. on Numerical and Physical Aspects of Aerodynamic Flows, California State University, Long Beach, January 21–24.*

SMITH, C. R., WALKER, J. D. A., HAIDARI, A. H. & SOBRUN, U. 1991 On the dynamics of near-wall turbulence. *Phil. Trans. R. Soc. Lond.* A **336**, 131–175.

VAN DEN BERG, B., ELSENAAR, A., LINDHOUT, J. P. F. & WESSELING, P. 1975 Measurements in an incompressible three-dimensional turbulent boundary layer, under infinite swept-wing conditions, and comparison with theory. *J. Fluid Mech.* **70**, 127–147.

WALKER, J. D. A., ABBOTT, D. E., SCHARNHORST, R. K. & WEIGAND, G. G. 1989 A wall-layer model for the velocity profile in turbulent flows. *AIAA J.* **27**, 140–149.

WALKER, J. D. A., ECE, M. C. & WERLE, M. J. 1991 An embedded function approach for turbulent flow prediction. *AIAA J.* **29**, 1810–1818.

WALKER, J. D. A. & STEWARTSON, K. 1974 Separation and the Taylor column for a hemisphere. *J. Fluid Mech.* **66**, 767–789.

WIE, Y.-S. & DeJARNETTE, F. R. 1988 Numerical investigation of three-dimensional separation using the boundary-layer equations. *AIAA Paper* 88-0617, *26th Aerospace Sciences Meeting, Reno, Nevada.*

YAJNIK, K. S. 1970 Asymptotic theory of turbulent shear flows. *J. Fluid Mech.* **42**, 411–427.

YUHAS, L. J. & WALKER, J. D. A. 1982 An optimization technique for the development of two-dimensional steady turbulent boundary layer models. *Rep.* FM-1. Dept. Mech. Eng. and Mech., Lehigh Univ.; also *AFOSR*-TR-0417.